Talanta 245 (2022) 123450

Contents lists available at ScienceDirect

Talanta

journal homepage: www.elsevier.com/locate/talanta

Photoreduced Ag^+ surrounding single poly(4-cyanostyrene) nanoparticles for undifferentiated SERS sensing and killing of bacteria

Ya-Qin Liu [a,1], Wei Zhu [a,b,1], Quan Yuan [a,**], Ji-Ming Hu [a], Xin Zhang [c], Ai-Guo Shen [a,b,*]

[a] College of Chemistry and Molecular Sciences, Wuhan University, Wuhan, 430072, PR China
[b] Research Center of Graphic Communication, Printing and Packaging, Wuhan University, Wuhan, 430079, PR China
[c] Beijing Digital Sky Eye Biotechnology Co., Beijing, 100089, PR China

ARTICLE INFO

Keywords:
SERS
Bacteria
Undifferentiated sensing and killing
Silver ions
Photoreduction

ABSTRACT

Developing a rapid, low cost and sensitive sensing strategy for undifferentiated detection and fast killing of bacterial pathogens are critical to alleviating bacteria infections. Here, we propose a direct photoreduction method to synthesize the SERS tag by integrating poly(4-cyanostyrene) nanoparticles (NPs) and silver ions, which are applied as bio-sensing system for bacteria sensing and fast killing. Under a focused laser spot, silver ions on the surface of the poly(4-cyanostyrene) NPs could be photoreduced into Ag NPs, thereby causing the Raman signal amplification of poly(4-cyanostyrene) NPs up to 40 times, and there is a good linear correlation between the Raman intensity of poly(4-cyanostyrene) NPs and different concentrations of Ag^+. Moreover, 4-mercaptophenylboronic acid, performing the same recognition function for both the Gram-positive and Gram-negative bacteria, is used as bridge between the bacteria and Ag^+ by the inherent chemical bonding. Based on further constructed bio-sensing system, we achieved the quick count and killing of both Gram-positive bacteria, *e.g.*, *Staphylococcus aureus* (*S. aureus*), and Gram-negative bacteria, *e.g.*, *Escherichia coli* (*E. coli*). Notably, the sensing strategy can detect at least ~100 cells of *E. coli*, ~10 cells of *S. aureus* and ~10 cells of their mixture in less than 40 min. The detection accuracy for actual samples can also reach over 80% and the bacteria were entirely killed by Ag^+ after the detection, avoiding bacterial contamination in the environment. This novel method is anticipated to perform as a simple yet effective tool for fast and sensitive bacteria counting and killing.

1. Introduction

Various pathogenic microorganisms have caused a widespread and important public health threat [1–4]. As few as 100 cells of *Escherichia coli* (*E. coli*) can result in severe illness and even fatal infections due to their strong vitality and rapid reproduction [5–7]. Therefore, the rapid, sensitive, and undifferentiated sensing method for quantifying bacterial cells plays an increasingly important role in multiple areas, such as disease prevention and safety supervision of drinking water and food [8–10]. Traditional culture-based methods, such as plate counting [11,12], are widely used for counting bacteria. However, these methods are particularly time-consuming (over 48 h), especially for slow-growing bacteria. The emerging methods based on enzyme-linked immunosorbent assay (ELISA) [13–15] and polymerase chain reaction (PCR) [16–18] are much faster than traditional methods. Regrettably, these technologies are still limited for point-of-care testing (POCT) by high cost, long time, low sensitivity, operational complexity, and strict experimental conditions.

Recently, developing advanced sensing strategies to fast acquire the number of bacteria has triggered researchers' wide attention. For example, fluorescent detection of metabolic molecule ATP [19,20] and "on-off" surface-enhanced Raman scattering (SERS) strategy based on the surface charge of bacteria might achieve fast bacterial quantification [21,22]. Nevertheless, bacteria below 1000 CFU/mL are difficult to be accurately judged by fluorescence detection due to the limitation of pM level detected ability (ATP content of each microbial cell is only fM). Moreover, the sensing detection based on surface charge will become inaccurate with the various size and shape of bacterial cells. To obtain the bacterial quantity timely with high sensitivity, several indirect SERS assays using triple-bond SERS tags that enabled the quantification of

* Corresponding author. College of Chemistry and Molecular Sciences, Wuhan University, Wuhan, 430072, PR China.
** Corresponding author.
E-mail addresses: yuanquan@whu.edu.cn (Q. Yuan), agshen@whu.edu.cn (A.-G. Shen).
[1] Y. L. and W. Z. contributed equally to this manuscript.

https://doi.org/10.1016/j.talanta.2022.123450
Received 15 January 2022; Received in revised form 30 March 2022; Accepted 3 April 2022
Available online 6 April 2022

specific pathogenic bacteria at low concentrations (10 CFU/mL) have been developed based on noble metal nanoparticles (NPs) [1,23,24]. Regrettably, the detection time (usually over 2 h) is still a challenge to reach the high requirement of POCT, and the uncontrollable aggregation of nanomaterials and poor reproducibility are also the biggest challenge of indirect SERS detection for bacteria quantification. In parallel to detection, the timely killing of bacteria after detection is also critical in daily life and clinics. However, the current sensing methods are low-effective considering the prevention of bacterial contamination because they need an additional operation to kill the bacteria after detection. Therefore, a rapid, sensitive, and convenient technique for timely quantification and killing of pathogen bacteria is urgently needed. Ag^+ in terms of bacteria killing has attracted much attention because of its antibacterial activity, safety, and no drug resistance [25–27]. Furthermore, Ag^+ is sensitive to laser irradiation and has been demonstrated to be photoreduced to Ag NPs in the presence of organic matters such as pyridine [28], biotin [28], sodium citrate [29], thioxanthone [30]. and sodium alginate [31], because they tend to perform as the electron donor due to the strong oxidization of Ag^+ in the excited state.

Here, we suggested a sensing strategy of photoreduced silver ions on the surface of poly(4-cyanostyrene) NPs (poly(4CNS) NPs) as the SERS tags for indirect bacteria quantification and killing. In this concept, we confirmed that the Raman signal of poly(4CNS) NPs can be significantly enhanced with the increased concentration of Ag^+ under laser irradiation and there is a good linear correlation between them. Based on this, we designed a sensing method for bacteria quantification and chemical killing. As shown in Scheme 1, the bacteria were first incubated with the 4-mercaptophenylboronic acid (4-MPBA) solution at 37 °C for 15 min. In this way, enough 4-MPBA molecules were ensured to bound with both Gram-positive and Gram-negative bacteria based on the covalent bonds formed between the boronic acid group of 4-MPBA and the diol of peptidoglycan in bacterial cell walls, achieving the undifferentiated recognition to various bacteria [32–35]. Ag^+ solution was then added to the solution of 4-MPBA-treated bacteria to combine with –SH of 4-MPBA and kill the most of bacteria [36,37]. The difference in bacterial concentration resulted in the different amounts of residual Ag^+ in the supernate, which can be detected with poly(4CNS) NPs by Raman spectroscopy. Therefore, the sensing detection was achieved based on the good linear correlation between the Raman signal of poly(4CNS) NPs and bacteria concentration. The proposed method can achieve the counting of *E. coli*, *Staphylococcus aureus* (*S. aureus*) and their mixture as low as 100 CFU/mL, 10 CFU/mL, and 10 CFU/mL in 40 min, respectively. The detection accuracy of actual samples can reach over 80%, and the killing efficiency of this method can nearly reach 100%, which show a great potential for the future POCT and killing of bacteria.

2. Experimental section

2.1. Materials

The monomer of poly(4CNS) NPs, 4-cyanostyrene (C_9H_7N), was of 95% purity and was obtained from Aladdin Industrial Inc. (Shanghai, China). Potassium persulfate (KPS) was of 99% purity and was purchased from Sigma-Aldrich (U.S.A.). 4-MPBA was of 90% purity and was obtained by Sigma-Aldrich (U.S.A.). The metal ions used in this work, including silver nitrate ($AgNO_3$), lead chloride ($PbCl_2$), ferrous sulfate ($FeSO_4·7H_2O$), aluminum sulfate octadecahydrate ($Al_2(SO_4)_3·18H_2O$), copper dinitrate ($Cu(NO_3)_2·3H_2O$), sodium chloride (NaCl), potassium chloride (KCl), manganese sulfate ($MnSO_4·H_2O$), nickel chloride hexahydrate ($NiCl_2·6H_2O$), zinc sulfate heptahydrate ($ZnSO_4·7H_2O$), magnesium sulfate heptahydrate ($MgSO_4·7H_2O$), Calcium chloride anhydrous ($CaCl_2$), and Cobalt Chloride ($CoCl_2·6H_2O$) were of analytical grade and were provided by Sinopharm Chemical Reagent Co., Ltd. (Shanghai, China). The tryptone and yeast extract used for preparing Luria−Bertani (LB) broth were both obtained from Sinopharm Chemical Reagent Co., Ltd. (Shanghai, China). The deionized water (18.2 MΩ/cm) used throughout the experiment was supplied by the Millipore-Q purification system.

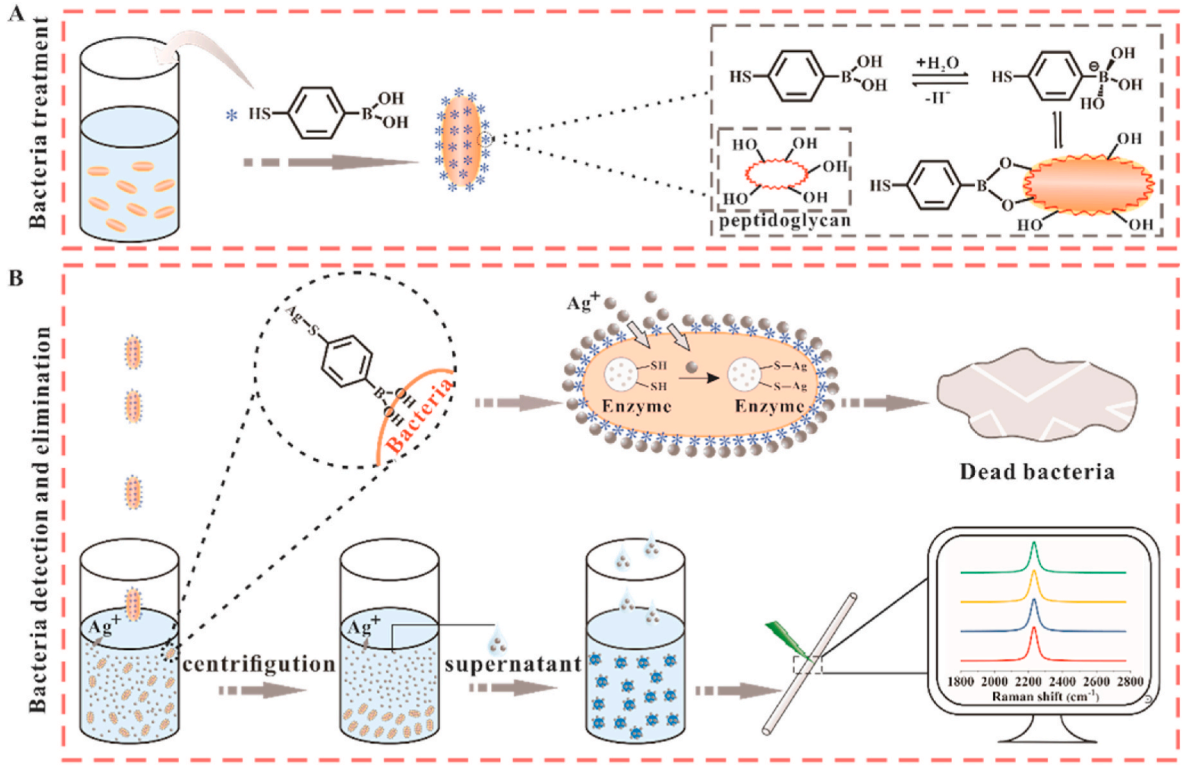

Scheme 1. Conceptual illustration of the constructed method for microbial detection and killing.

2.2. Bacteria culture

E. coli DSM 4230 and *S. aureus* ATCC 91093 used in this study were purchased from China Center for Type Culture Collection. All bacterial strains were cultured in sterile LB broth at 37 °C with continuous shaking at 180 rpm/min until the bacteria concentration was up to 1×10^7 CFU/mL. Afterward, the two initial bacteria solutions were first collected by centrifuging at 4000 rpm for 5 min at room temperature and then cleaned three times with deionized water before resuspending in the deionized water. Prior to the preparation of the test bacteria sample, the bacteria concentration was determined via the plating and culturing method.

2.3. Preparation and characterization of poly(4CNS) NPs

Poly(4CNS) NPs were synthesized via the emulsion polymerization method without a saponifier. The details were described as follows. 0.05 g of 4-cyanostyrene was added into a 50 mL three-necked round-bottomed flask, and then 10 mL of water was added at room temperature. The mixture was then vigorously stirred at room temperature for 30 min. Afterward, the 0.6 mL of KPS aqueous solution was added to induce the reaction under the protection of nitrogen when the oil bath was heated to 70 °C. The poly(4CNS) NPs were obtained after continuous heating and stirring for another 2 h. The obtained polymer solution was naturally cooled down to room temperature and was further purified for one week via dialysis using a dialysis bag with a molecular weight of 3500 Da. The purified polymers were preserved at 4 °C for further use. The weight of 1 mL poly(4CNS) NPs was measured after drying at 40 °C overnight by an electronic balance (AL104, Mettler-Toledo, Shanghai, China) and the weight of 1 mL poly(4CNS) NPs was 2.4 mg. Gel permeation chromatography (GPC) was used to obtain the molecular weight distribution of the poly(4CNS) NPs by Agilent PL-GPC50. During the detection, a liquid chromatography system equipped with a UV–vis detector was used. Sample pretreatment refers to our previous work [38], the freeze-dried samples were dissolved with DMSO before being injected into the detection system. The morphology images of polymers were recorded by a ZEISS field-emission scanning electron microscope (FESEM) operating at 5 kV. The element characterization of polymers was carried out by SEM equipped with X-ray energy-dispersion spectroscopy (EDS) operating at 15 kV. Dynamic light scattering (DLS) and zeta potential were both measured using a Malvern Nano-ZSP90 instrument.

2.4. Quantitative analysis of Ag^+ solution using Poly(4CNS) NPs

A series of Ag^+ solutions with ten different concentrations were prepared in deionized water for quantitative evaluation. The detail concentrations are 300 μM, 600 μM, 900 μM, 1200 μM, 1500 μM, 1800 μM, 2100 μM, 2400 μM, 2700 μM and 3000 μM. Poly(4CNS) NPs at the concentration of 2.4 mg/mL and the different concentrations of Ag^+ solutions were mixed with equal volume so that the final detected concentration of the Ag^+ ion solutions were 150 μM, 300 μM, 450 μM, 600 μM, 750 μM, 900 μM, 1050 μM, 1200 μM, 1350 μM and 1500 μM. The mixture was blended by vortex (MX-S Mixers, Scilogex, USA) and detected by Raman spectroscopy (Renishaw, UK). Each measurement was repeated at least three times. The calibration curve of Ag^+ was performed by plotting the Raman intensity of poly(4CNS) NPs at the Raman shift of 2233 cm^{-1} versus the different concentrations of Ag^+ through Origin software. The images of the different mixtures were captured by a Canon camera.

2.5. Detection selectivity experiment of metal ions

The aqueous solutions of different metal ions, including $AgNO_3$, $PbCl_2$, $FeSO_4{\cdot}7H_2O$, $Al_2(SO_4)_3{\cdot}18H_2O$, $Cu(NO_3)_2{\cdot}3H_2O$, NaCl, KCl, $MnSO_4{\cdot}H_2O$, $NiCl_2{\cdot}6H_2O$, $ZnSO_4{\cdot}7H_2O$, $MgSO_4{\cdot}7H_2O$, $CaCl_2$, and $CoCl_2{\cdot}6H_2O$, were prepared with the concentration of 2 mM at room temperature. Afterward, 100 μl of poly(4CNS) NPs at the concentration of 2.4 mg/mL was mixed with 100 μl of the different metal ion solutions so that the final detected concentration of the metal ion solution was 1 mM. The mixture was blended by vortex and detected by Raman spectroscopy. The different Raman intensity of poly(4CNS) NPs at the Raman shift of 2233 cm^{-1} caused by different metal ions was displayed as a histogram through Origin software. The images of the different mixtures were captured by a Canon camera.

2.6. Bacteria quantification using poly(4CNS) NPs

Based on the counting results, the two bacteria solutions (*E. coli* and *S. aureus*) were firstly diluted to 1×10^7 CFU/mL, and then the bacteria cells were collected by centrifuging at 4000 r/min for 5 min. The bacteria mixture was prepared of *E. coli* and *S. aureus* with the ratio of 1:3. 1 mM of 4-MPBA solution was prepared in ethanol (EtOH). 100 μl 4-MPBA solution and 900 μl ddH_2O were added to resuspend the collected bacteria and the resuspended bacteria solution was incubated at 37 °C for 15 min. Next, the bacteria solution was centrifuged at 4000 r/min for 5 min and the excess 4-MPBA was removed. The bacteria cells were finally resuspended in deionized water and serially diluted to different concentrations as experimental groups, including 1×10^7 CFU/mL, 1×10^6 CFU/mL, 1×10^5 CFU/mL, 1×10^4 CFU/mL, 1×10^3 CFU/mL, 1×10^2 CFU/mL and 1×10^1 CFU/mL. Afterwards, 500 μl of bacteria solution at different concentrations was mixed with 500 μl of the Ag^+ ion solution at the concentration of 4 mM. The mixture was incubated for 2 min at room temperature and then centrifuged at 4000 r/min for 5 min. Afterward, 100 μl of the supernate was blended with 100 μl of poly(4CNS) NPs at the concentration of 2.4 mg/mL and detected by Raman spectroscopy. The calibration curve of *E. coli*, *S. aureus*, and their mixture was performed by plotting the Raman intensity of poly(4CNS) NPs at the Raman shift of 2233 cm^{-1} versus the different concentrations of the *E. coli*, *S. aureus*, and their mixture through Origin software.

2.7. Raman measurements and data processing

SERS measurements were carried out on a Renishaw *inVia* confocal Raman microscope spectrometer equipped with a 532 nm laser unless otherwise specified. The Raman spectra were acquired with glass capillary using a 20 × long-working-distance objective lens with a laser spot of 1.6 μm. For the Raman spectra over a spectral range from 1800 to 2800 cm^{-1}, they were collected once with the integration time of 5 s and laser energy of 40 mW. For the Raman spectra over a spectral range from 600 to 2800 cm^{-1}, they were collected once with the integration time of 10 s and laser energy of 20 mW. The Raman spectra were then subtracted baseline and smoothed by commercial WIRE 3.4 software. The fitting mode is selected as “Intelligent fitting”, polynomial order as 11, and noise tolerance as 1.50.

2.8. Wide detection of bacteria in drinking water, lake water, and sour milk beverage

The drinking water and sour milk beverage were obtained from a local supermarket. The lake water was obtained from the East Lake Scenic Area of Wuhan. Target bacteria with unknown concentrations were added to the drinking water. There was no other additional operation for sour milk beverage and lake water except dilution before detection. Then, the method constructed in this article was applied to evaluate the feasibility according to the general procedure. The accuracy of the bacteria detection in real samples with our method was estimated by comparing it with culturing results.

3. Result and discussion

3.1. Synthesis and characterization of poly(4CNS) NPs

The effective Raman reporters were prepared with 4-cyanostyrene as the monomer via traditional emulsion polymerization, possessing unique Raman scattering in the biological Raman silent region (1800-2800 cm^{-1}) where nearly all biomolecules do not produce Raman scattering signals [39,40]. As shown in Fig. 1A and Table S1, the 4-cyanostyrene molecules were polymerized to produce a polymer with the relative molecular weight of 20761. The cyano groups of the poly(4CNS) NPs render them unique Raman scattering (2227 cm^{-1}) in the Raman silent region according to the Raman spectrum in Fig. 1A. Moreover, the Raman peak of poly(4CNS) NPs had a high signal-to-noise ratio (S/N > 5), and no other Raman background signals were observed in the Raman silent region. FESEM was employed to capture the morphology images of poly(4CNS) NPs (Fig. 1B). As shown, poly(4CNS) NPs exhibited a uniform spherical shape with the size of 140 nm, which was consistent with the average hydrodynamic size measured by DLS. The reconstructed histograms shown in Fig. 1C and Fig. S1 indicated the narrow size distributions and low polydispersity index (PDI = 0.029) of poly(4CNS) NPs, further suggesting the uniform size of poly(4CNS) NPs. The component of poly(4CNS) NPs was shown in EDS mapping that C and N elements originated from poly(4CNS) NPs, the existing silicon (Si) and platinum (Pt) elements originated from silicon slice and ion beam sputtering apparatus, respectively (Fig. S2).

Zeta potential is normally applied to evaluate the stability of the colloid particles. The further zeta potential experiments demonstrated that the poly(4CNS) NPs were negatively charged with the zeta potential of −26.2 mV, illustrating the outstanding stability of the polymers in water (Fig. S3). The long-term stability of the Raman reporter elected as Raman signal output is essential for improving the accuracy and reproducibility of quantification SERS analysis. Therefore, the stability of poly(4CNS) NPs was evaluated keeping at room temperature for different times (i.e., 0, 1, 2, 3, and 4 weeks) by FESEM, DLS, and Raman spectroscopy. It is shown that very few changes in the morphologies of poly(4CNS) NPs were found during a month (Fig. 1B and Fig. S4), and there were no obvious differences in terms of the average size of poly(4CNS) NPs as the DLS measurement shown (Fig. S5). In addition, the Raman signal of poly(4CNS) NPs was monitored by an *invia* Raman spectroscopy equipped with a 532 nm laser. As shown in Fig. S6 and Fig. S7, the constant Raman intensity of poly(4CNS) NPs can be obtained due to their excellent uniformity and stability. The outstanding homogeneity and stability of poly(4CNS) NPs indicate its potential as an outstanding Raman reporter for sensing detection.

3.2. The Raman signal enhancement of poly(4CNS) NPs based on the photoreduction of Ag^+

Interestingly, it has been demonstrated in this article that Ag^+ can be photoreduced to Ag NPs in presence of poly(4CNS) NPs, thus achieving the Raman signal enhancement of the poly(4CNS) NPs. To demonstrate this process, $AgNO_3$ solution and the mixed solution of $AgNO_3$ and poly(4CNS) NPs were irradiated with the 532-nm laser of 40 mW for 30 min. As shown in Fig. S8, the color of the mixed solution of $AgNO_3$ and poly(4CNS) NPs has changed to yellow after laser irradiation, while there was no obvious change for $AgNO_3$ solution. Moreover, the SEM images further showed that many Ag NPs were produced in the mixed solution of $AgNO_3$ and poly(4CNS) NPs, while the $AgNO_3$ solution alone did not have any obvious changes, demonstrating poly(4CNS) NPs performed as the electron donor in the photoreduction process of Ag^+. It is because Ag^+ will be excited to an excited state under 532-nm laser irradiation, endowing them with strong oxidation. In addition, the dense electron cloud of the cyano group reduces the electron cloud density of the

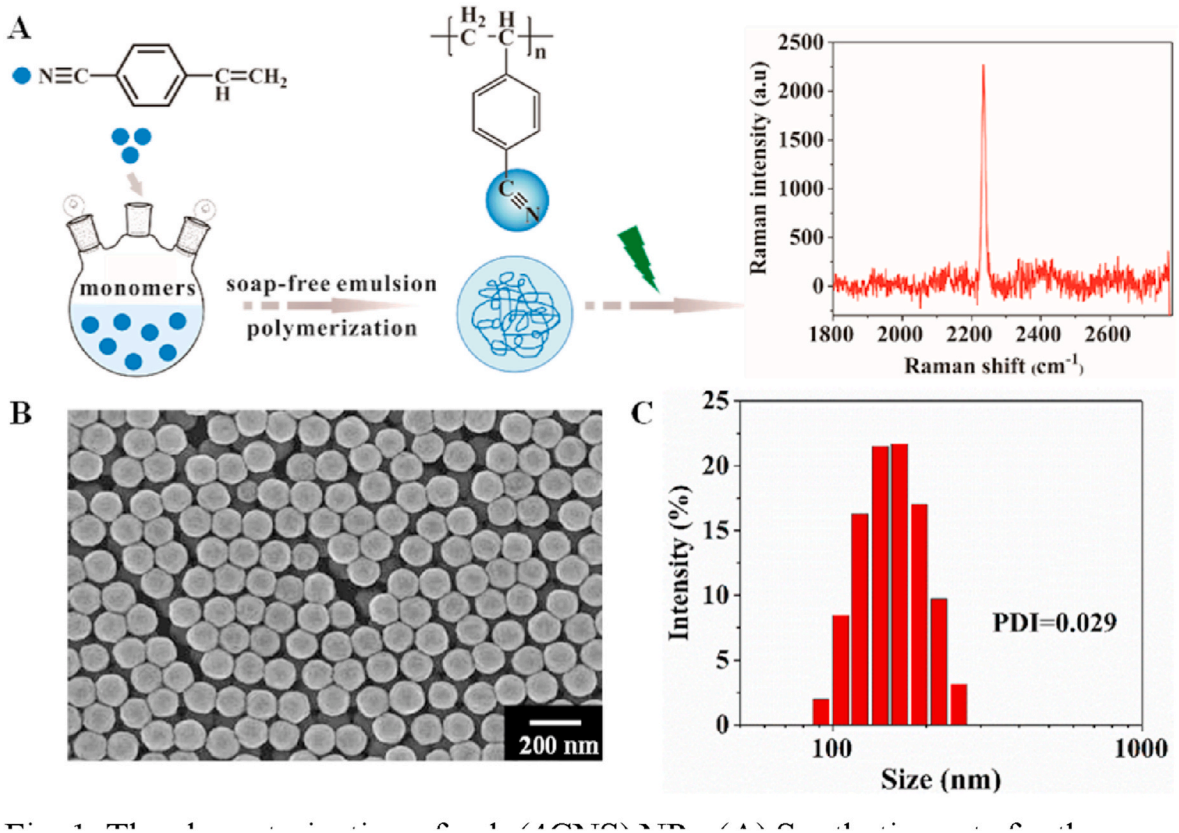

Fig. 1. The characterization of poly(4CNS) NPs. (A) Synthetic route for the preparation of poly(4CNS) NPs and the Raman spectra of poly(4CNS) NPs (B) Representative SEM image of poly(4CNS) NPs. (C) DLS profiles of poly(4CNS) NPs, the polydispersity index (PDI) is 0.029.

benzene ring in the structure of poly(4CNS) NPs so that the poly(4CNS) NPs are might lose the electron [41], thus resulting in the formation of Ag^0 (Fig. 2A) [31,42]. Also, the complexation interaction between Ag^+ and the cyano group facilitated electron transport. Finally, the aggregation of Ag^0 contributes to the formation of Ag NPs surrounding the negatively-charged poly(4CNS) NPs, causing the significant Raman signal enhancement of poly(4CNS) NPs.

To further explore the possible Raman signal enhancement of poly (4CNS) NPs caused by the photoreduction of Ag^+, Raman spectra of poly (4CNS) NPs with and without the addition of Ag^+ aqueous solution were detected and analyzed. As shown in Fig. S9, the Raman signal of poly (4CNS) NPs has been significantly enhanced with the addition of Ag^+ using a 532 nm laser as an exciting laser, demonstrating the photoreduction of Ag^+ to Ag NPs. Two Raman spectra of the polymers are nearly the same with and without the addition of Ag^+ at the Raman shift of 1175 and 1607 cm^{-1}, indicating that Ag^+ did not interact with vinyl groups and phenyl ring. Differently, the Raman shift of cyano group in poly(4CNS) NPs shifted from 2227 cm^{-1}–2233 cm^{-1} after adding the Ag^+, thus it is proved that the evident red-shift phenomenon was commonly observed because of the complexation interaction between the Ag^+ and the C≡N, which is consistent with the previous study [43–45]. Laser irradiation condition was further explored for the photoreduction of Ag^+ to Ag NPs, FESEM and TEM images were captured to observe the morphologic change of poly(4CNS) NPs with Ag^+ under different irradiation conditions (Fig. 2B–G). As shown in Fig. 2B–C and E-F, there are no obvious particles on the surface of poly (4CNS) NPs under dark condition or natural light. It is because photon energy must exceed a certain critical value to initiate the reduction reaction, the dark condition or natural light with low energy cannot excite the electrons in the poly(4CNS) NPs so they do little contribution to the photoreduction process of Ag^+ [46]. On the contrary, many NPs were produced on the surface of poly(4CNS) NPs with 532-nm laser irradiation and the size of these NPs was approximately 5 nm. It was further confirmed that these NPs were Ag NPs by the EDS mapping and XRD spectrum (Fig. S10 and Fig. S11). Ag element is mainly derived from the NPs on the polymer in the EDS mapping. In the XRD spectrum, the diffraction peak positions of the NPs on the polymers can be attributed to the standard Ag cubic phase (JCPDS 04 to 0783). Additionally, 38.2°, 44.3°, 64.4°, and 77.5° are corresponded to the crystal planes of (111), (200), (220), and (311) of Ag NPs, respectively [47–49]. However, there are no obvious changes in the Raman spectra of poly(4CNS) NPs with or without Ag^+ when a 633 nm laser was used (Fig. S12). Although the reason for this is still unclear, it is clear poly(4CNS) NPs are a powerful Raman reporter for Ag^+ detection using a 532 nm laser rather than a 633 nm laser. Therefore, a 532 nm laser was used for the subsequent experiment.

The irradiation time plays a vital role in the production of Ag NPs, directly influencing the signal enhancement of poly(4CNS) NPs. Therefore, the solution of poly(4CNS) NPs and Ag^+ were irradiated with 532-nm laser for different times before detection, including 0 min, 5 min, 10 min, 15 min, 20 min, 25 min, and 30 min (Fig. S13 and Fig. S14). Afterward, the mixed solution was detected with an integration time of 5 s and laser energy of 40 mW. As shown, the Raman intensity decreased with the increase of the irradiation time because of the instability of Ag NPs after the long-time irradiation. Moreover, many Ag NPs can be observed on the polymers by FESEM measurement, illustrating the cause of the high SERS enhancement (Fig. S15). Notably, enough Ag NPs and the highest Raman signals can be produced due to the laser irradiation conducted by integration time of 5 s during the detection process, which does not need the additional laser irradiation before detection. Therefore, the mixed solution of poly(4CNS) NPs and Ag^+ are detected directly with Raman spectroscopy in the subsequent experiment without

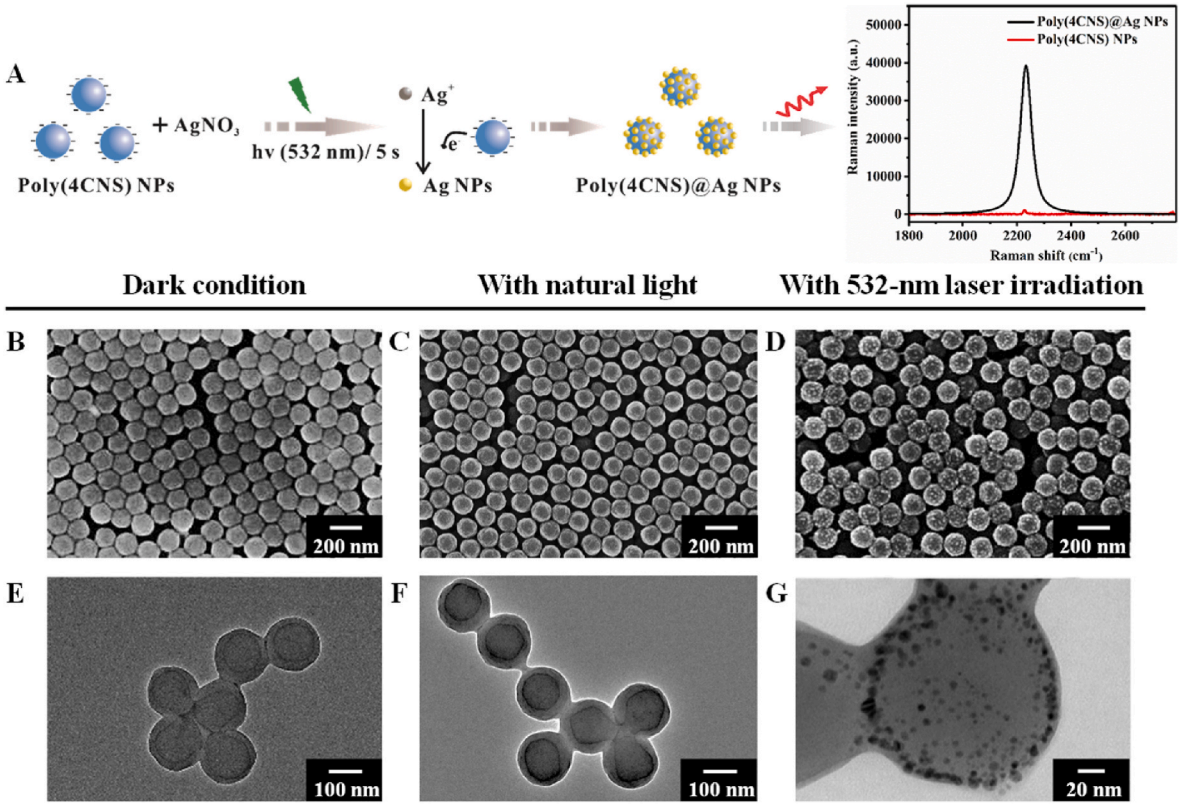

Fig. 2. The illustration of photoreduced silver ions on the surface of poly(4CNS) NPs (A), and the SEM and TEM images of poly(4CNS) NPs and Ag^+ under different conditions: (B) SEM images of poly(4CNS) NPs and Ag^+ under dark condition, (C) SEM images of poly(4CNS) NPs and Ag^+ with natural light, (D) SEM images of poly (4CNS) NPs and Ag^+ with 532-nm laser irradiation; (E) TEM images of poly(4CNS) NPs and Ag^+ under dark condition, (F) TEM images of poly(4CNS) NPs and Ag^+ with natural light, (G) TEM images of poly(4CNS) NPs and Ag^+ with 532-nm laser irradiation.

the additional irradiation before detection, making the detection process simpler and faster.

To elucidate the possible relation between the Raman signal of the poly(4CNS) NPs and the concentration of Ag^+, different concentrations of Ag^+ solution were added into the poly(4CNS) NPs solution. The appearance, DLS, and Raman spectra of the mixture were measured and analyzed. As shown in Fig. S16 and Fig. S17, the appearance and the average size of the poly(4CNS) NPs had no apparent difference with the addition of various concentrations of Ag^+ solution before the laser irradiation, suggesting the poly(4CNS) NPs is not affected by Ag^+ and the polymers are still stable. The calibration curve shown in Fig. 3A and the Raman spectra shown in Fig. 3B exhibited a good linear correlation between the concentration of Ag^+ and the Raman intensity of poly (4CNS) NPs at the concentration over the range from 300 μM to 1050 μM with R^2 of 0.9831. The RSD% for each measurement also illustrated the good accuracy and reproducibility of our measurements (Table S2). Moreover, the FESEM images shown in Fig. S18 exhibited that more Ag NPs were photoreduced with the increased concentration of Ag^+ solution, accounting for the signal increase of poly(4CNS) NPs with the increased concentration of Ag^+ solution. Our results showed that poly (4CNS) NPs performed very well as a promising Raman reporter for Ag^+ quantitative analysis.

3.3. Detection selectivity experiment of metal ions

Poly(4CNS) NPs had uniform size, excellent stability, unique Raman scattering, and abundant functional cyano groups, which could promote the complexation interaction between poly(4CNS) NPs and metal ions. Therefore, poly(4CNS) NPs were expected to own outstanding detection capability for metal ions by Raman spectroscopy. In order to explore the detection selectivity of poly(4CNS) NPs for Ag^+, the detection capabilities of poly(4CNS) NPs were investigated for different metal ions including Pb^{2+}, Zn^{2+}, Ni^+, Mg^{2+}, Mn^{2+}, Na^+, K^+, Cu^{2+}, Fe^{2+}, Ca^{2+}, Co^{2+}, Al^{3+}, and Ag^+. As shown in Fig. S19, the appearance of poly (4CNS) NPs showed no obvious change after adding different metal ions. It is noted that all the mixtures were still colloidal solution without flocculation, suggesting that poly(4CNS) NPs were still stable in presence of different metal ions. The histogram between Raman intensity of poly(4CNS) NPs and different metal ions was constructed by Origin software (Fig. 3C) and the representative Raman spectra collected from the poly(4CNS) NPs with different metal ions were shown in Fig. 3D, displaying that the significantly enhanced Raman signal can be only collected from poly(4CNS) NPs with the addition of Ag^+ under the laser irradiation of 532 nm. It is maybe contributed to the good photoactivity of Ag^+ so that Ag^+ can be photoreduced as Ag NPs. Our results demonstrated the detection specificity of poly(4CNS) NPs for Ag^+.

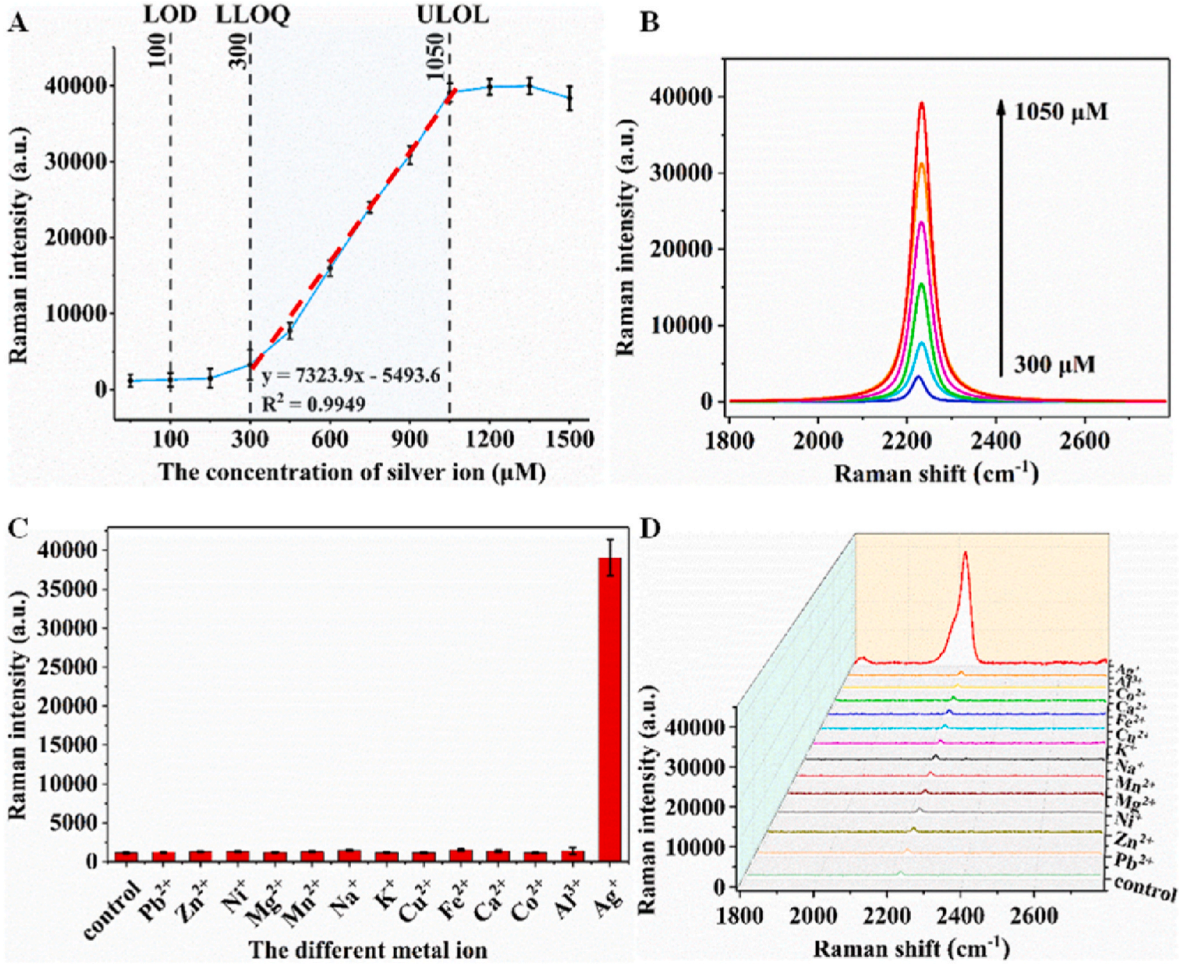

Fig. 3. The detection selectivity of poly(4CNS) NPs for different metal ions. (A) The dynamic range of linearity for detection of different concentrations of Ag^+ solution using poly(4CNS) NPs as Raman signal output. Abbreviations: LOD, the limit of detection; LLOQ, the lower limit of quantitation; ULOL, the upper limit of linear response. (B) Selected Raman spectra showing the quantitative analysis for Ag^+ solution with different concentrations. (C) The Raman intensity of poly(4CNS) NPs after the addition of different metal ions. (D) The representative Raman spectra were obtained from poly(4CNS) NPs after the addition of different metal ion. Error bars: the standard deviation of three independent experiments.

3.4. Detection and killing of E. coli, S. aureus, and their mixture

E. coli as a representative of gram-negative bacteria is a common water-borne and foodborne pathogen, which can cause many diseases such as enteritis, peritonitis, cholecystitis, and appendicitis. Meanwhile, *S. aureus* as a representative of gram-positive bacteria is a human commensal that can also cause serious systemic infections, such as dermatitis, gastroenteritis, and toxic shock syndrome. Bacteria counting

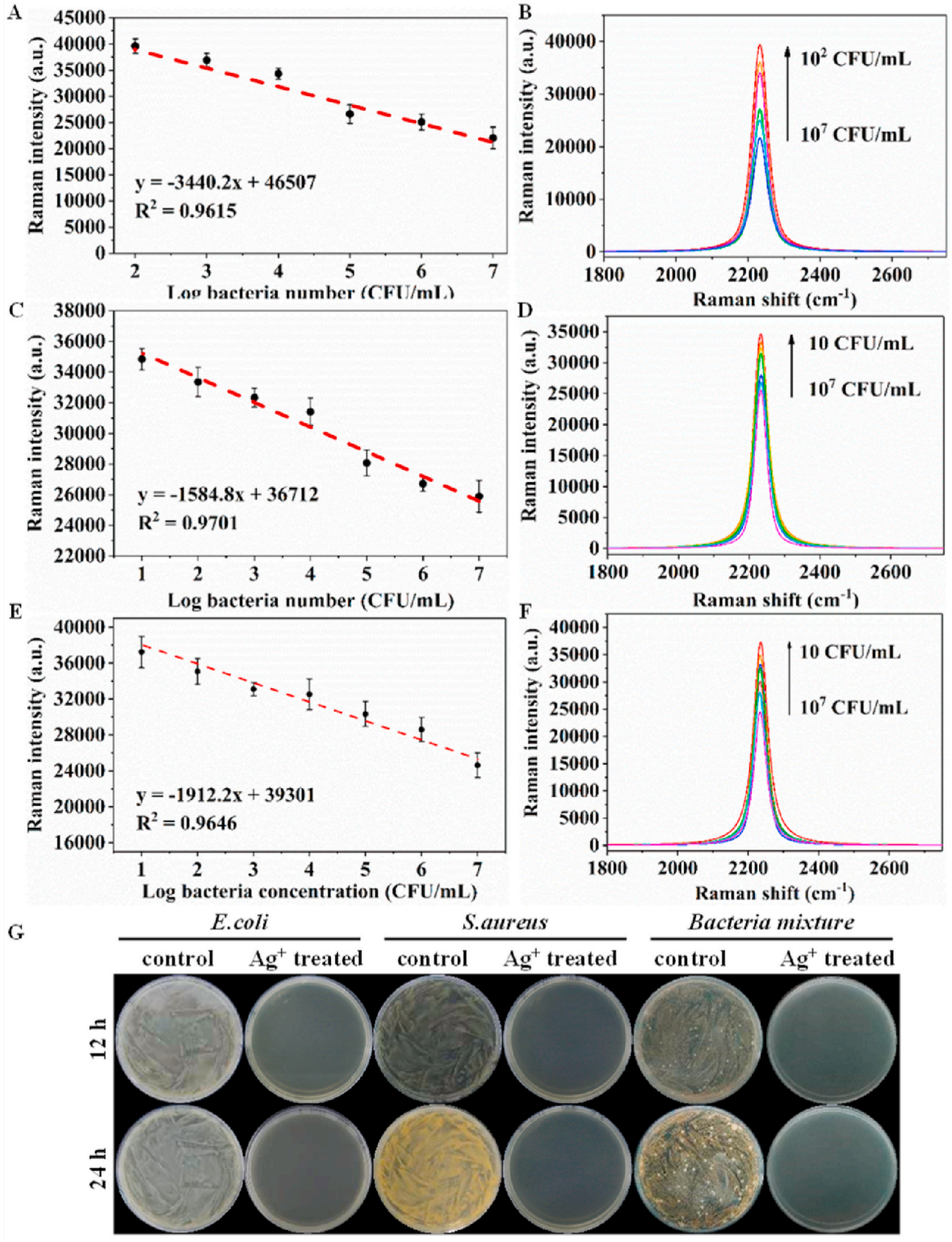

Fig. 4. Sensitivity of the developed method for the detection of *E.coli*, *S. aureus* and their mixture. The calibration curve between Raman intensity of poly(4CNS) NPs and various concentrations of *E.coli* (A), *S. aureus* (C) and the mixture of *E. coli* and *S. aureus* (E). The representative Raman spectra of poly(4CNS) NPs for the various concentration of *E.coli* (B), *S. aureus* (D) and the mixture of *E. coli* and *S. aureus* (F). Error bars: the standard deviation obtained from three independent experiments. The killing of bacteria after detection. (G) The *E. coli*, *S. aureus* and their mixture treated with and without Ag^+ were cultured on agar plates for 12 h and 24 h.

is vital for disease prevention and human healthcare. To investigate the feasibility of this method for bacteria quantification analysis, we chose *E. coli* and *S. aureus* as the representative bacteria for the quantification analysis. A series of *E. coli* and *S. aureus* (10–10^7 CFU/mL) solutions treated by 4-MPBA solution were blending with 4 mM of Ag^+ solution, and the residual Ag^+ that was not combined with –SH was further blending with poly(4CNS) NPs and detected by Raman spectroscopy. As shown in Fig. 4A and Fig. 4B, the Raman intensity at 2233 cm^{-1} of poly (4CNS) NPs decreased with the increased concentration of *E. coli* at the concentration of 10^2–10^7 CFU/mL. Similarly, the Raman intensity at 2233 cm^{-1} of poly(4CNS) NPs also decreased as the *S. aureus* concentration increased at the concentration of 10–10^7 CFU/mL (Fig. 4C and D). It is because more Ag^+ was adsorbed on 4-MPBA-treated bacteria and less Ag^+ remained in the supernate when the concentration of the bacteria increased. The calibration curves between the obtained Raman intensity of poly(4CNS) NPs and the concentration of *E. coli* and *S. aureus* were constructed by Origin software (Fig. 4A and C). It was shown that there was a good linear correlation between the Raman intensity of poly (4CNS) NPs and the concentration of the bacteria, the calibration curve for *E. coli* was $y = -3440.2x+46507$ with R^2 of 0.9615, achieving LLOQ as low as 100 CFU/mL, and the calibration curve for *S. aureus* was $y = -1584.8x+36712$ with R^2 of 0.9701, achieving LLOQ as low as 10 CFU/mL. In addition, the feasibility of this method for the quantification of the bacteria mixture of *E. coli* and *S. aureus* was also investigated. As shown in Fig. 4E and F, the Raman intensity at 2233 cm^{-1} of poly(4CNS) NPs also decreased as the bacteria mixture concentration increased, and a good linear correlation between the Raman intensity of poly(4CNS) NPs and the concentration of the bacteria mixture was established ($y = -1912.2x+39301$, $R^2 = 0.9646$). Notably, the bacteria inhibition capability of our method was also explored by the usage of the plating and culturing method. As presented in Fig. 4G, it was observed that numerous *E. coli*, *S. aureus* and their mixture were in the control group. However, the number of *E. coli* and *S. aureus* both decreased significantly in the presence of Ag^+, and nearly all the bacteria were killed. All these results confirm that the bacteria quantification method mentioned in this article has high sensitivity and accuracy for *E. coli* and *S. aureus* detection, and is effective for bacteria inhibition.

3.5. Detection and killing of complex bacteria samples in the actual sample

In addition to standard bacterial solution sensing from artificial preparation, wide detection of numerous bacterial strains existing in actual samples has attracted more and more attention to guarantee environmental safety for a high-quality life. To this end, the feasibility of the detection method constructed in this article was further explored by employing it for the detection of spiked bacteria mixtures in drinking water. The linear calibration curve ($y = -1912.2x+39301$, $R^2 = 0.9646$) between Raman intensity of poly(4CNS) NPs and various concentrations of the bacteria mixture was used to obtain the bacteria concentration in the drinking water. As shown in Fig. 5, for the three parallel trials, our method provided consistent results with an accuracy of 80%, which have a good match with the number measured by the culture method. The complex components in sour milk beverages and lake water especially for saccharides and some organic molecules with the negative charge will influence the recognition of 4-MPBA to bacteria and the adsorption of silver ions, increasing the detection difficulty. Based on the procedure in our method, the sour milk beverages and lake water were first centrifuged to collect the bacteria before the subsequent operation, avoiding the interferences existing in actual samples. The linear calibration curve ($y = -3440.2x+46507$, $R^2 = 0.9615$) and ($y = -1912.2x+39301$, $R^2 = 0.9646$) were used to obtain the lactobacillus concentration in the sour milk beverage and bacteria concentration in the lake water, respectively. As shown in Table S3, the detected concentration of bacteria in lake water and sour milk based on our method is comparable to the cultural method with the relative recovery of 114% and 115%, respectively. The errors were maybe caused by the inhomogeneous adsorption of various bacteria to Ag^+ and the potential impurities also influenced our results. Moreover, the detected concentration of bacteria in actual samples can be relatively consistent for the repeated measurements with the RSD% less than 10%, demonstrating the great potential of our method for water monitoring and food safety monitoring. Compared to the long detection time (>24 h) of bacterial culture, the whole process of our method can be completed within 40 min, meeting the time requirements of clinical POC sensing. Furthermore, the bacteria have been entirely killed after detection, avoiding the second environmental pollution (Fig. S20). Although it is demonstrated that wide bacteria detection in actual samples with high sensitivity and time efficiency would become more convenient based on our method soon, it is still a challenge for the simple sample pretreatment of the actual samples to satisfy the detection requirements and the detection accuracy still need to be improved to overcome the complexity of the actual samples.

4. Conclusion

In this work, it is demonstrated that the Raman signal of poly(4CNS) NPs can be specifically enhanced up to 40 times by the photoreduction of Ag^+, and there was a good linear correlation with the $R^2 = 0.9831$ between the concentration of Ag^+ and the Raman intensity of poly (4CNS) NPs over the range from 300 to 1050 μM. Based on the interesting phenomena, a rapid, highly sensitive, and free bacteria

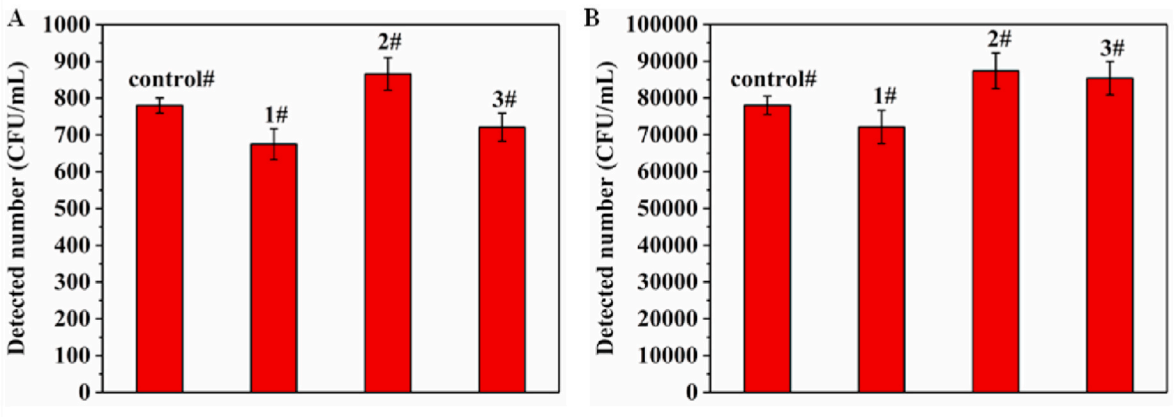

Fig. 5. Detected numbers of the spiked bacteria mixture of *E. coli* and *S. aureus* in drinking water for three parallel bacteria samples by the method proposed in this article. Control# group represents the result detected by the plating and culturing method.

contamination method was successfully developed for quantification of *E. coli*, *S. aureus* and their mixture in the standard solution, which can be also used for the bacteria sensing in the actual sample with the accuracy of 80%. Furthermore, the bacteria can be effectively killed, avoiding bacteria contamination after the bacteria detection. In the future, the development of effective target molecules which can achieve more specific recognition to both Gram-positive and negative bacteria as well as the simpler and faster method for sample pretreatment will further improve the accuracy and the work efficiency of our method. In a word, this novel strategy provides a kind of universal quantitative detection and timely killing method for microorganism research.

Credit author statement

Yaqin Liu: Investigation, Formal analysis, Writing an original draft, Visualization. Wei Zhu: Methodology, Formal analysis, Validation. Quan Yuan: Resources. Jiming Hu: Resources. Xin Zhang: Writing – review & editing, GPC measurement, Aiguo Shen: Supervision, Resources, Writing – review & editing, Funding acquisition.

Declaration of competing interest

The authors declare that they have no known competing financial interests or personal relationships that could have appeared to influence the work reported in this paper.

Acknowledgment

This work was financially supported by the National Natural Science Foundation of China (Nos. 22074109, 21874102, and 21775114) and China Postdoctoral Science Foundation (2021M702506). We thank Dr. Xiaodong Zhou from Core Facility of Wuhan University for his assistance with the FESEM analysis.

Appendix A. Supplementary data

Supplementary data to this article can be found online at https://doi.org/10.1016/j.talanta.2022.123450.

References

[1] L. Bi, X. Wang, X. Cao, L. Liu, C. Bai, Q. Zheng, J. Choo, L. Chen, SERS-active Au@Ag core-shell nanorod (Au@AgNR) tags for ultrasensitive bacteria detection and antibiotic-susceptibility testing, Talanta 220 (2020) 121397.
[2] J.A. Kim, D.J. Wales, A.J. Thompson, G.Z. Yang, Fiber-optic SERS probes fabricated using two-photon polymerization for rapid detection of bacteria, Adv. Opt. Mater. 8 (9) (2020) 1901934.
[3] H. Lee, H. Han, S. Jeon, Baleen-mimicking virtual filters for rapid detection of pathogenic bacteria in water using magnetic nanoparticle chains and a Halbach ring, ACS Sens. 5 (11) (2020) 3432–3437.
[4] Y. Liu, H. Zhou, Z. Hu, G. Yu, D. Yang, J. Zhao, Label and label-free based surface-enhanced Raman scattering for pathogen bacteria detection: a review, Biosens. Bioelectron. 94 (2017) 131–140.
[5] S. Hameed, L. Xie, Y. Ying, Conventional and emerging detection techniques for pathogenic bacteria in food science: a review, Trends Food Sci. Technol. 81 (2018) 61–73.
[6] Y. Liu, A. Gilchrist, J. Zhang, X.F. Li, Detection of viable but nonculturable Escherichia coli O157:H7 bacteria in drinking water and river water, Appl. Environ. Microbiol. 74 (5) (2008) 1502–1507.
[7] A. Zhu, S. Ali, Y. Xu, Q. Ouyang, Q. Chen, A SERS aptasensor based on AuNPs functionalized PDMS film for selective and sensitive detection of Staphylococcus aureus, Biosens. Bioelectron. 172 (2021) 112806.
[8] N. Elgiddawy, S. Ren, A. Yassar, A. Louis-Joseph, H. Sauriat-Dorizon, W.M.A. El Rouby, A.O. El-Gendy, A.A. Farghali, H. Korri-Youssoufi, Dispersible conjugated polymer nanoparticles as biointerface materials for label-free bacteria detection, ACS Appl. Mater. Interfaces 12 (36) (2020) 39979–39990.
[9] S. Sharifi, S.Z. Vahed, E. Ahmadian, S.M. Dizaj, A. Eftekhari, R. Khalilov, M. Ahmadi, E. Hamidi-Asl, M. Labib, Detection of pathogenic bacteria via nanomaterials-modified aptasensors, Biosens. Bioelectron. 150 (2020) 111933.
[10] H. Wang, H. Ceylan Koydemir, Y. Qiu, B. Bai, Y. Zhang, Y. Jin, S. Tok, E.C. Yilmaz, E. Gumustekin, Y. Rivenson, A. Ozcan, Early detection and classification of live bacteria using time-lapse coherent imaging and deep learning, Light Sci. Appl. 9 (2020) 1–17.
[11] S. He, X. Hong, M. Zhang, L. Wu, X. Yan, Label-free detection of bacteria in fruit juice by nano-flow cytometry, Anal. Chem. 92 (3) (2020) 2393–2400.
[12] O. Scheler, N. Pacocha, P.R. Debski, A. Ruszczak, T.S. Kaminski, P. Garstecki, Optimized droplet digital CFU assay (ddCFU) provides precise quantification of bacteria over a dynamic range of 6 logs and beyond, Lab Chip 17 (11) (2017) 1980–1987.
[13] S.Y. Choi, G.E. Rhie, J.H. Jeon, Development of a double-antibody sandwich ELISA for sensitive detection of Yersinia pestis, Microbiol. Immunol. 64 (1) (2020) 72–75.
[14] B. Pang, C. Zhao, L. Li, X. Song, K. Xu, J. Wang, Y. Liu, K. Fu, H. Bao, D. Song, X. Meng, X. Qu, Z. Zhang, J. Li, Development of a low-cost paper-based ELISA method for rapid Escherichia coli O157:H7 detection, Anal. Biochem. 542 (2018) 58–62.
[15] K. Pei, Y. Xiong, B.L. Xu, K.S. Wu, X.M. Li, J. Hu, Y.H. Xiong, Colorimetric ELISA for ochratoxin A detection based on the urease-induced metallization of gold nanoflowers, Sensor. Actuator. B Chem. 262 (2018) 102–109.
[16] K.D. Clark, J.A. Purslow, S.A. Pierson, O. Nacham, J.L. Anderson, Rapid preconcentration of viable bacteria using magnetic ionic liquids for PCR amplification and culture-based diagnostics, Anal. Bioanal. Chem. 409 (21) (2017) 4983–4991.
[17] S. Petralia, S. Conoci, PCR technologies for point of care testing: progress and perspectives, ACS Sens. 2 (7) (2017) 876–891.
[18] J. Vidic, P. Vizzini, M. Manzano, D. Kavanaugh, N. Ramarao, M. Zivkovic, V. Radonic, N. Knezevic, I. Giouroudi, I. Gadjanski, Point-of-Need DNA testing for detection of foodborne pathogenic bacteria, Sensors-Basel 19 (5) (2019) 1100.
[19] N. Duan, W. Sun, S. Wu, L. Liu, X. Hun, Z. Wang, Aptamer-based F0F1-ATPase biosensor for Salmonella typhimurium detection, Sensor. Actuator. B Chem. 255 (2018) 2582–2588.
[20] M. Shamsipur, K. Molaei, F. Molaabasi, S. Hosseinkhani, A. Taherpour, M. Sarparast, S.E. Moosavifard, A. Barati, Aptamer-based fluorescent biosensing of adenosine triphosphate and cytochrome c via aggregation-induced emission enhancement on novel label-free DNA-capped silver nanoclusters/graphene oxide nanohybrids, ACS Appl. Mater. Interfaces 11 (49) (2019) 46077–46089.
[21] L.F. Tadesse, C.S. Ho, D.H. Chen, H. Arami, N. Banaei, S.S. Gambhir, S.S. Jeffrey, A. A.E. Saleh, J. Dionne, Plasmonic and electrostatic interactions enable uniformly enhanced liquid bacterial surface-enhanced Raman scattering (SERS), Nano Lett. 20 (10) (2020) 7655–7661.
[22] H. Zhou, D. Yang, N.P. Ivleva, N.E. Mircescu, R. Niessner, C. Haisch, SERS detection of bacteria in water by in situ coating with Ag nanoparticles, Anal. Chem. 86 (3) (2014) 1525–1533.
[23] X. Bai, A.G. Shen, J.M. Hu, A sensitive SERS-based sandwich immunoassay platform for simultaneous multiple detection of foodborne pathogens without interference, Anal. Methods 12 (40) (2020) 4885–4891.
[24] X. Gao, Y. Yin, H. Wu, Z. Hao, J. Li, S. Wang, Y. Liu, Integrated SERS platform for reliable detection and photothermal elimination of bacteria in whole blood samples, Anal. Chem. 93 (3) (2021) 1569–1577.
[25] L. Gao, Y. Wang, Y. Li, M. Xu, G. Sun, T. Zou, F. Wang, S. Xu, J. Da, L. Wang, Biomimetic biodegradable Ag@Au nanoparticle-embedded ureteral stent with a constantly renewable contact-killing antimicrobial surface and antibiofilm and extraction-free properties, Acta Biomater. 114 (2020) 117–132.
[26] Y. Xu, X. Liu, Y. Zheng, C. Li, K.W. Kwok Yeung, Z. Cui, Y. Liang, Z. Li, S. Zhu, S. Wu, Ag_3PO_4 decorated black urchin-like defective TiO_2 for rapid and long-term bacteria-killing under visible light, Bioact. Mater. 6 (6) (2021) 1575–1587.
[27] M. Zhu, X. Liu, L. Tan, Z. Cui, Y. Liang, Z. Li, K.W. Kwok Yeung, S. Wu, Photo-responsive chitosan/Ag/MoS_2 for rapid bacteria-killing, J. Hazard Mater. 383 (2020) 121122.
[28] A.M. Ahern, R.L. Garrell, In situ photoreduced silver nitrate as a substrate for surface-enhanced Raman spectroscopy, Anal. Chem. 59 (23) (1987) 2813–2816.
[29] R. Sato-Berrú, R. Redón, A. Vázquez-Olmos, J.M. Saniger, Silver nanoparticles synthesized by direct photoreduction of metal salts. Application in surface-enhanced Raman spectroscopy, J. Raman Spectrosc. 40 (4) (2009) 376–380.
[30] G.S. Batibay, O.T. Gunkara, N. Ocal, N. Arsu, In-situ photoinduced formation of self–assembled Ag NPs using POSS-TX as nano-photoinitiator in PEGMEA/PEGDA polymer matrix and creating self-wrinkled pattern, J. Photochem. Photobiol., A 359 (2018) 73–79.
[31] T. Sato, S. Kuroda, A. Takami, Y. Yonezawa, H. Hada, Photochemical formation of silver-gold (Ag@Au) composite colloids in solutions containing sodium alginate, Appl. Organomet. Chem. 5 (1991) 261–268.
[32] J. Huang, J.H. Sun, A.R. Warden, X.T. Ding, Colorimetric and photographic detection of bacteria in drinking water by using 4-mercaptophenylboronic acid functionalized AuNPs, Food Control 108 (2020) 106885.
[33] H. Wang, Y. Zhou, X. Jiang, B. Sun, Y. Zhu, H. Wang, Y. Su, Y. He, Simultaneous capture, detection, and inactivation of bacteria as enabled by a surface-enhanced Raman scattering multifunctional chip, Angew. Chem. Int. Ed. 54 (17) (2015) 5132–5136.
[34] K. Xu, R. Zhou, K. Takei, M. Hong, Toward flexible surface-enhanced Raman scattering (SERS) sensors for point-of-care diagnostics, Adv. Sci. 6 (16) (2019) 1900925.
[35] X. Zhou, Z. Hu, D. Yang, S. Xie, Z. Jiang, R. Niessner, C. Haisch, H. Zhou, P. Sun, Bacteria detection: from powerful SERS to its advanced compatible techniques, Adv. Sci. 7 (23) (2020) 2001739.
[36] L. Cheng, Z.W. Cai, T.J. Ye, X.H. Yu, Z.J. Chen, Y.F. Yan, J. Qi, L. Wang, Z.H. Liu, W.G. Cui, L.F. Deng, Injectable polypeptide-protein hydrogels for promoting infected wound healing, Adv. Funct. Mater. 30 (25) (2020) 2001196.
[37] X.H. Pan, L.X. Fu, H. Wang, Y. Xue, J.H. Zu, Synthesis of novel sulfydryl-functionalized chelating adsorbent and its application for selective adsorption of Ag(I) under high acid, Separ. Purif. Technol. 271 (2021) 118778.

[38] W. Zhu, E.L. Cai, H.Z. Li, P. Wang, A.G. Shen, J. Popp, J.M. Hu, Precise encoding of triple-bond Raman scattering of single polymer nanoparticles for multiplexed imaging application, Angew. Chem. Int. Ed. 60 (40) (2021) 21846–21852.
[39] L. Jing, X. Liang, Z. Deng, S. Feng, X. Li, M. Huang, C. Li, Z. Dai, Prussian blue coated gold nanoparticles for simultaneous photoacoustic/CT bimodal imaging and photothermal ablation of cancer, Biomaterials 35 (22) (2014) 5814–5821.
[40] W. Zhu, M.Y. Gao, Q. Zhu, B. Chi, L.W. Zeng, J.M. Hu, A.G. Shen, Monodispersed plasmonic Prussian blue nanoparticles for zero-background SERS/MRI-guided phototherapy, Nanoscale 12 (5) (2020) 3292–3301.
[41] C.C. Price, Substitution and orientation in the benzene ring, Chem. Rev. 29 (1) (1941) 37–67.
[42] V. Kumar, D.K. Singh, S. Mohan, R.K. Gundampati, S.H. Hasan, Photoinduced green synthesis of silver nanoparticles using aqueous extract of Physalis angulata and its antibacterial and antioxidant activity, J. Environ. Chem. Eng. 5 (1) (2017) 744–756.
[43] T. Shoeib, H.E. Aribi, K.W.M. Siu, A.C. Hopkinson, A study of silver (I) ion-organonitrile complexes: ion structures, binding energies, and substituent effects, J. Phys. Chem. A 105 (4) (2001) 710–719.
[44] X.X. Yao, W.J. Zhang, J.L. Huang, Z.W. Du, X.K. Hong, X.F. Chen, X.L. Hu, X. H. Wang, Enhanced photocatalytic nitrogen fixation of Ag/B-doped g-C_3N_4 nanosheets by one-step in-situ decomposition-thermal polymerization method, Appl. Catal. A-Gen. 601 (2020) 117647.
[45] Q. Zhang, Y.Y. Chai, M.T. Cao, F.L. Yang, L. Zhang, W.L. Dai, Facile synthesis of ultra-small Ag decorated g-C_3N_4 photocatalyst via strong interaction between Ag^+ and cyano group in monocyanamide, Appl. Surf. Sci. 503 (2020) 143891.
[46] Y. Yonezawa, T. Sato, S. Kuroda, Photochemical formation of colloidal silver: peptizing action of acetone ketyl radical, J. Chem. Soc., Faraday Trans. 87 (12) (1991) 1905–1910.
[47] K. Ma, P. Dong, M. Liang, S. Yu, Y. Chen, F. Wang, Facile assembly of multifunctional antibacterial nanoplatform leveraging synergistic sensitization between silver nanostructure and vancomycin, ACS Appl. Mater. Interfaces 12 (6) (2020) 6955–6965.
[48] X. Peng, S.G. Karakalos, W.E. Mustain, Preferentially oriented Ag nanocrystals with extremely high activity and faradaic efficiency for CO_2 electrochemical reduction to CO, ACS Appl. Mater. Interfaces 10 (2) (2018) 1734–1742.
[49] S.K. Sen, T.C. Paul, S. Dutta, M.N. Hossain, M.N.H. Mia, XRD peak profile and optical properties analysis of Ag-doped h-MoO_3 nanorods synthesized via hydrothermal method, J. Mater. Sci. Mater. Electron. 31 (2) (2019) 1768–1786.